Channel Estimation for Filtered OFDM Transceiver Systems

Ali Baghaki, Benoit Champagne
Department of Electrical and Computer Engineering, McGill University, 3480 University Street
Montreal, QC, Canada, H3A 0E9
Email: ali.baghaki@mail.mcgill.ca; benoit.champagne@mcgill.ca

***Abstract*—The advantages of filtered orthogonal frequency division multiplexing (f-OFDM) over conventional OFDM, universally filtered multicarrier (UFMC) and filter bank multicarrier (FBMC) techniques have made it a prominent choice for the future generations of wireless networks. Nevertheless, due to its backward compatibility, the specific task of channel estimation for f-OFDM systems has not yet been addressed; although, due to the difference in the signal model, by doing so one might achieve improvements in the performance or spectral efficiency of the system. We develop a pilot-aided channel estimation scheme for f-OFDM with no or minimal cyclic prefix (CP) based on the statistical properties of the interference, i.e. inter-symbol interference (ISI), inter-carrier interference (ICI), adjacent-carrier interference (ACI) and noise terms. We demonstrate the possibility to shorten or totally remove the CP from the f-OFDM transceiver while applying a one-tap-per-subcarrier equalizer and maintaining the performance and complexity of the transceiver system satisfactory. We propose a pilot-based least square (LS) estimator and an average-taking modified variant of it that perform very close to the perfect channel and outperform a pilot-to-pilot interpolation-based channel estimator in BER simulations.**

I. Introduction

Among the proposed multicarrier modulation (MCM) techniques that have gained significant attention for future generation of wireless networks is filtered orthogonal frequency division multiplexing (filtered OFDM or f-OFDM). Filtered OFDM is one of the two main proposed waveforms that apply subband filtering in contrast to filter bank multicarrier (FBMC) techniques and conventional OFDM that make up the two ends of the spectrum in terms of usage of filters per frequency band; the former applying a filter per subcarrier and the latter deploying none. Hence, the main advantage of subband-filtered waveforms over the conventional OFDM is in their diminished out-of-band leakage while their prominent advantage over FBMC techniques lies in lower latency and complexity and superior multiple input multiple output (MIMO) compatibility [1].

Moreover, unlike universally filtered multicarrier (UFMC) technique as another form of subband filtered multicarrier waveforms, in f-OFDM, the filter length is allowed to exceed the cyclic prefix (CP) length to achieve a better balance between the frequency and time localization. This is while in UFMC the subband filter length is limited to the CP length in order to avoid inter symbol interference (ISI). Instead, in f-OFDM, the ISI incurred due to the extended filter length can be limited since the main energy of the filter is confined within its main lobe in the time domain. The extended filter length in f-OFDM also helps to design a filter with an acceptable pass-band distortion. Finally, it has been mentioned that due to the use of the CP, the channel equalization in the proposed f-OFDM has lower complexity than in UFMC [2].

One should note, however, that the specific task of channel estimation for f-OFDM systems has not yet been considered in the literature. Although this is due to the overall nice backward compatibility of the f-OFDM system as compared to the other post-OFDM waveforms, e.g. FBMC, the observations in [3] especially that of the relatively unchanged ISI level with respect to the CP length, show that, potentially, addressing the channel estimation and equalization task for f-OFDM can enhance the performance of the system beyond what is achieved by simply employing the schemes developed for OFDM.

In light of this observation, we note that although f-OFDM is superior to OFDM in terms of out-of-band leakage, it employs a CP per subband to ease the task of channel equalization [4]. In this work, we aim to demonstrate the possibility to shorten or totally remove the CP while applying merely a one-tap-per-subcarrier equalizer and maintaining the performance and complexity of the transceiver system acceptable. To this end, we utilize the observations of [3] and those of ours to appropriately model the interference terms, i.e. ISI, inter-carrier interference (ICI) and adjacent carrier interference (ACI), and develop a pilot-based channel estimation method.

We consider a synchronized downlink SISO link; however, extension of the same method to MIMO scenarios is possible. It is worth noting that the described estimation in the downlink may be used both in a closed-loop manner, where the base station (BS) transmits the training sequence and receives the user's feedback to compute and, possibly, pre-equalize the channel, and in an open loop link where the user(s) can compute and equalize the corresponding channel(s) by using the known training sequence [5]. As will be seen from the results, the potential to shorten or remove the CP length compared to the previous works is fulfilled by effectively removing some of the interference through the proposed channel estimation method.

II. System Model

Fig. 1 depicts the downlink f-OFDM transceiver system as implemented in this work. Only three adjacent subbands at the transmitter side and one at the receiver side are shown. This block diagram is similar to that in [3] with minor

This research was funded by the Natural Sciences and Engineering Research Council (NSERC) of Canada.

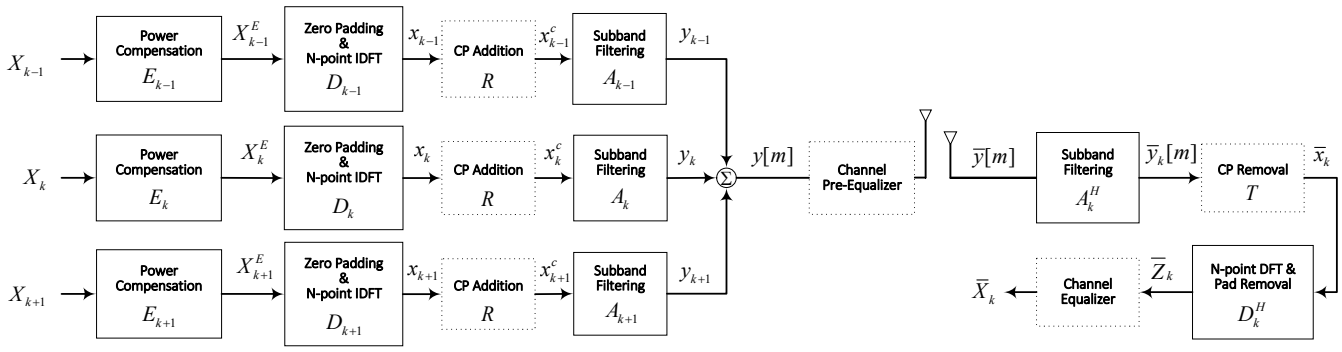

Fig. 1: Transceiver model of a downlink f-OFDM system; three adjacent subbands are shown at the transmitter and one at the receiver

modifications pertained to the contributions of this work. Specifically, the CP addition and removal blocks are dashed because our aim is to minimize the CP length or totally remove it. In addition, possibility of pre-equalization at the transmitter side, is illustrated. These points will be further clarified once the proposed channel estimation and compensation scheme is described in Section III.

As seen in Fig. 1, on the BS side, the main processing stages per subband are power compensation, zero padding and N-point inverse discrete Fourier transform (IDFT), possible CP addition and subband filtering which are followed by superposition of all subband signals. Using the matrix-vector representation of [3] where all operations (e.g. convolution, DFT, IDFT) are represented by matrix multiplication, we denote these subband operations by E_k, D_k, R and A_k respectively. On the receiver side, aside from the power compensation, the dual of other subband operations are performed which are represented by A_k^H, T, D_k^H where the superscript $[.]^H$ indicates the hermitian operation.

At a given time index in the transmitter input, for each subband, a modulated symbol vector of size $M\times 1$ is fed to the transceiver where M represents the number of subcarriers per subband. The total transmitted symbol over all subbands can be shown as

$$X = [X_1^T, X_2^T, ..., X_K^T]^T \in \mathbb{C}^{N\times 1} \tag{1}$$

where

$$X_k = [X_k(1), X_k(2), ..., X_k(M)]^T \in \mathbb{C}^{M\times 1} \tag{2}$$

is the transmitted signal over the k-th subband, K is the number of subbands, and we assume $E\{X_k(i)^2\} = 1$, for $i = 0, 1, ..., M-1$. The total number of subcarriers is $N = M\times K$. In the first processing step, as proposed in [3], the variations in the power boost and suppression at different subcarriers are taken into the account and compensated. This slight power imbalance is due to the subband filtering at the transmitter and receiver.

The power-compensated vector is then zero-padded to size $N\times 1$ over which the N-point normalized IDFT is performed. In a conventional f-OFDM system, the CP is prepended to the resulting vector followed by subband filtering. Due to the ISI produced by the overlapping of filter tails with the adjacent f-OFDM symbols in time domain, the subband signal can be represented by addition of a desired component and an ISI-producing one[1]. As such, in matrix-vector form, the resulting subband signals before transmission can be written as

$$y_k = y_k^{DES} + y_k^{ISI} \tag{3}$$

where

$$y_k^{DES} = A_k R D_k E_k X_k \tag{4}$$
$$y_k^{ISI} = y_k^P + y_k^N \tag{5}$$
$$y_k^P = A_k R D_k E_k X_k^P \tag{6}$$
$$y_k^N = A_k R D_k E_k X_k^N \tag{7}$$

where, in turn, X_k^P and X_k^N denote the previous and next input f-OFDM symbols respectively; hence, the corresponding transmitted signal components y_k^P and y_k^N. In (6), E_k is the $M\times M$ convolution matrix for power compensation, $D_k \in \mathbb{C}^{N\times M}$ is the $[(k-1)M+1]$-th to the (kM)-th columns of the N-point IDFT convolution matrix D given by $D(\nu,\mu) = \frac{1}{\sqrt{N}} e^{j2\pi\nu\mu/N}$, and $R = [\mathbf{0}_{L_{CP}\times(N-L_{CP})}, \mathbf{I}_{L_{CP}}; \mathbf{I}_N]$ is the CP prepending matrix. Defining the impulse response of the filter at the k-th subband as $\mathbf{a}_k = [a_k(0), a_k(1), ..., a_k(L_f-1)]$ and denoting one symbol duration as $L_{SYM} = N+L_{CP}$, the subband filtering operation is represented by A_k, which is a $(L_{SYM}+L_f-1)\times L_{SYM}$ Toeplitz matrix where $[\mathbf{a}_k, \mathbf{0}_{1\times(L_{SYM}-1)}]^T$ and $[a_k(0), \mathbf{0}_{1\times(L_{SYM}-1)}]$ define its first column and first row respectively. The subband signals are then summed up to form the baseband signal

$$y[m] = \sum_{k=1}^{K} y_k[m], \qquad m = 1, 2, ..., N \tag{8}$$

which is upconverted and transmitted.

The received signal is filtered, per subband, by a matched subband filter A_k^H which is the para-conjugate of the corresponding transmit subband filter. Next, any existing CP is removed, represented by multiplication by $T = [\mathbf{0}_{N\times L_{CP}}, \mathbf{I}_N]$, and the resulting vector is converted to frequency domain by an N-point DFT from which the transmitted $M\times 1$ vector is extracted according to the location of the subband on the

[1]Herein, we use the term 'f-OFDM symbol' at the low sampling rate and 'symbol' at the high rate.

total bandwidth. This operation is written as multiplication by D_k^H and is followed by channel equalization according to [3]. Defining the channel impulse response (CIR) between the BS and the subband k as $\mathbf{h}_k = [h_k(0), h_k(1),..., h_k(L_{h,k}-1)]$, the channel effect is represented as multiplication by the Toeplitz matrix $\mathbf{H}_k \in \mathbb{C}^{(L_{SYM}+L_{h,k}+L_f-2)\times(L_{SYM}+L_f-1)}$ with $[h_k(1), \mathbf{0}_{1\times(L_{SYM}+L_f-2)}]$ and $[\mathbf{h}_k, \mathbf{0}_{1\times(L_{SYM}+L_f-L_{h,k}-2)}]^T$ defining the first row and first column respectively. The received symbol at the k-th subband in the most general form of the interference terms contains components of ISI, ICI, ACI and noise since the condition of interference-free communication formulated in [3], i.e. $L_{CP} \geq L_{h,k}+2L_f-3$, is not met. Hence, the received signal at the subband k before equalization reads as

$$\bar{Z}_k = \bar{Z}_k^{DES}+\bar{Z}_k^{ISI}+\bar{Z}_k^{ACI}+\bar{Z}_k^{ICI}+n_k \tag{9}$$

where n_k denotes the subband noise contribution and other terms represent the desired, ISI, ACI and ICI contributions to the subband symbol respectively. The end-to-end effect of ISI is modeled as multiplication of the previous and next f-OFDM symbols by matrices of the same size that only contain the first L_s and the last $L_{h,k}+L_f-2-L_s$ rows of $\mathbf{H}_k$ respectively and are zero otherwise. These matrices are given by $\mathbf{H}_k^N = [(\mathbf{0}_{(L_{SYM}-L_s)\times L_{SYM}})^T, (H_k^N)^T]^T$ and $\mathbf{H}_k^P = [(H_k^P)^T, (\mathbf{0}_{(L_{SYM}-L_{h,k}-L_f+L_s+2)\times L_{SYM}})^T]^T$, where H_k^N and H_k^P represent the first L_s rows and the last $L_{h,k}+L_f-2-L_s$ rows of $\mathbf{H}_k$ respectively. In contrast, the desired component of the received symbol $\bar{Z}_k^{DES}$ is the result of multiplication by the central part of $\mathbf{H}_k$ denoted as $\mathbf{H}_k^C$ being of size $L_{SYM}\times(L_{SYM}+L_f-1)$ and containing the rows between the foregoing components of the channel matrix. As such, the desired and the ISI components of the received subband symbol is written as

$$\bar{Z}_k^{DES} = D_k^H T A_k^H \mathbf{H}_k^C y_k^{DES} \tag{10}$$
$$\bar{Z}_k^{ISI} = \bar{Z}_k^P+\bar{Z}_k^N \tag{11}$$
$$\bar{Z}_k^P = D_k^H T A_k^H \mathbf{H}_k^P y_k^P \tag{12}$$
$$\bar{Z}_k^N = D_k^H T A_k^H \mathbf{H}_k^N y_k^N \tag{13}$$

where the superscripts $[.]^P$ and $[.]^N$ indicate the received ISI components related to the previous and the next symbol respectively. In the general form, the subbands might be asynchronous with a time offset of τ_i between the subband of interest and the i-th subband. However, due to the non-orthogonality between the subbands, even if the they are synchronous, the ACI component exists. Each subband can overlap with up to three f-OFDM symbols of the other one belonging to the next, the current and the previous time indexes, i.e. y_i^N, y_i^C and y_i^P. Respectively, these three terms correspond to the three parts of the channel convolution matrix, H_k^1, H_k^2 and H_k^3, which take the first $L_s+\tau_i$ rows, the rows number $(L_s+\tau_i+1)$ to $(L_s+\tau_i+L_{SYM})$, and the rows number $L_s+\tau_i+L_{SYM}+1$ to $\tau_i+L_{SYM}+L_{h,k}+L_f-2$ of $\mathbf{H}_k$. As such, defining $\mathbf{H}_k^1 = [(H_k^1)^T, (\mathbf{0}_{(L_{SYM}-L_{h,k}-L_f+L_s+\tau_i+2)\times L_{SYM}})^T]^T$, $\mathbf{H}_k^2 = H_k^2$, and $\mathbf{H}_k^3 = [(\mathbf{0}_{(L_{SYM}-L_s-\tau_i)\times L_{SYM}})^T, (H_k^3)^T]^T$, we have

$$\bar{Z}_k^{ACI} = D_k^H T A_k^H \sum_{\substack{i=1,\\ i\neq k}}^{K} (\mathbf{H}_k^1 y_i^N+\mathbf{H}_k^2 y_i^C+\mathbf{H}_k^3 y_i^P) \tag{14}$$

To compute the ICI term caused by one-tap equalization, it is noted that if the aforementioned condition on interference-free communication was met, the ICI would not exist with one-tap equalization. Hence, the ICI component can be computed as the difference in the received symbol between when the CP is long enough to fully avoid ICI and when it is not. Letting the minimum length of CP to avoid interference be L_O, the full size CP insertion matrix is $R_O = [(\mathbf{0}_{L_O\times(N-L_O)}, \mathbf{I}_{L_O})^T, \mathbf{I}_N^T]^T$ and the difference between full CP insertion and partial one is given by[2]

$$R_C = R_O-[(\mathbf{0}_{(L_O-L_{CP})\times N})^T, R^T]^T \tag{15}$$

or

$$R_C = \left[\begin{array}{c|c|c} \mathbf{0}_{(L_O-L_{CP})\times(N-L_O)} & \mathbf{I}_{L_O-L_{CP}} & \mathbf{0}_{(L_O-L_{CP})\times L_{CP}} \\ \hline \multicolumn{3}{c}{\mathbf{0}_{(N+L_{CP})\times N}} \end{array}\right]. \tag{16}$$

In addition, we can show that, if $N = 2L_f$ as chosen in this work, removing the first $L_x = L_{h,k}+L_O-L_{CP}-2$ elements/rows results in a vector/matrix on which the N-point DFT can be performed; hence, $T_O = [\mathbf{0}_{N\times L_x}, \mathbf{I}_N]$[3]. Based on these definitions, [3] proves that

$$\bar{Z}_k^{ICI} = -D_k^H T_O A_k^H \mathbf{H}_k^C A_k R_C D_k E_k X_k \tag{17}$$

The power compensation matrix E_k is calculated by

$$E_k = (G_k^{[k]} F_k^{[k]})^{-1} (Q_k)^{\frac{1}{2}} \tag{18}$$

where

$$Q_k = \text{diag}(D_k^H T A_k^H A_k R D_k) \tag{19}$$
$$G_k^{[k]} = \text{diag}(g_k^{[k]}) \tag{20}$$
$$F_k^{[k]} = \text{diag}(f_k^{[k]}) \tag{21}$$

where in turn $g_k^{[i]}$ and $f_k^{[i]}$ are the matrices consisting of the $(i-1)M+1$ to the iM-th elements of g_k and f_k given by

$$f_k = D^H[\mathbf{a}_k, \mathbf{0}_{1\times(N-L_f)}]^T \tag{22}$$
$$g_k = D^H[\mathbf{c}_k, \mathbf{0}_{1\times(N-L_f)}]^T \tag{23}$$

and $c_k(m) = a_k(-m)^*$ for $m = 0,..., L_f-1$. The superscript $[.]^*$ denotes conjugate operation and performing diag[.] over a vector gives a diagonal matrix by using the operand as the main diagonal while over a square matrix extracts the main diagonal as the output vector.

Finally, $n_k = D_k^H T A_k^H \eta_k$ is the complex-valued subband noise vector after subband filtering, CP removal and DFT operation performed over η_k; the latter being an $M\times 1$ vector of additive white Gaussian noise symbols with zero mean and variance of σ_η^2.

[2]This implies that L_O cannot be greater than N and L_{CP} cannot be greater than L_O which means, e.g. for a typical choice of $L_f = \frac{N}{2}$, the ideal interference-free CP length given in [3] as $L_{h,k}+2L_f-3$ is not achievable. As such, this analytical ideal CP length is replaced by an empirical one that removes the interference effect to a practically ideal level and is obtained through simulations.

[3]Since the obtained analytical L_O by [3] does not work with typical value for L_f, we use the aforementioned empirical L_O in previous footnote and make sure $L_O-L_{CP} \geq 0$. This is how L_x is obtained in contrast to [3] where T_O is given as removing the first L_O elements.

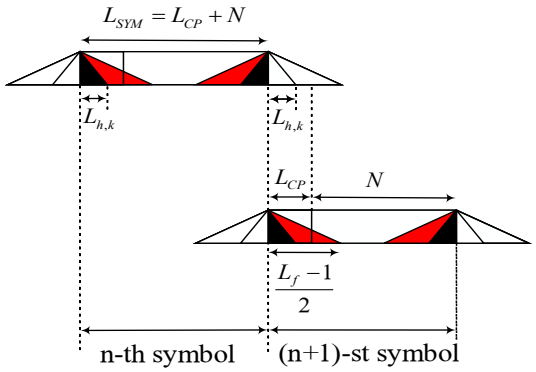

Fig. 2: ISI effect caused by subband filtering and channel.

III. Proposed Channel Estimation

Despite the conventional estimation methods for impairment sources in OFDM systems can be applied to f-OFDM and provide satisfactory results, one might be able to further improve the error rate performance or the spectral efficiency of the transceiver system if its specific signal model is exploited. To this end, the statistical properties of interference terms in this specific waveform need to be investigated. One way is to use the time-domain model of the transceiver system in Fig. 1, which is described in the next subsection.

A. Time-domain signal model

To derive the signal model of the f-OFDM system in Fig. 1, we begin with the transmitted symbol in one time index, of size $M\times 1$, on the k-th subband undergoing the power compensation as

$$X_k^E = E_k X_k \tag{24}$$

The power compensated symbol is then zero padded to the size $N\times 1$ and is called X_k^{pad}, where the zeros occupy non-data-bearing locations. The IDFT of the zero padded symbol, x_k, reads as

$$x_k[m] = \frac{1}{\sqrt{N}} \sum_{n=0}^{N-1} X_k^{pad}[n] e^{j2\pi nm/N}, m = 0, 1, ..., N-1. \tag{25}$$

After the possible CP insertion the resulting signal is

$$x_k^c = \Big[x_k[N-L_{CP}+1],\, x_k[N-L_{CP}+2], ..., \\ x_k[N], x_k[0], ..., x_k[N-1]\Big]^T, \tag{26}$$

which is filtered to obtain the subband signal before transmission.

Since overlapping of filter tails occurs at each stage where the convolution is performed, i.e. in subband filtering at the transmitter and receiver as well as in the channel, the resulting ISI length in the received f-OFDM symbol is $\frac{L_f-1}{2}$ from both sides adding up to L_f-1.[4] This is illustrated in Fig. 2. Assuming that the CIR is shorter than the subband filter's length, the overall ISI length per f-OFDM symbol is not altered by further filtering but is intensified by the channel effect and by the second subband filtering at the receiver.

[4]Without loss of generality, odd filter length, L_f, is assumed.

For the resulting f-OFDM symbol that is the addition of the desired component and the ISI components at the two ends, we can write

$$y_k[m] = y_k^{DES}[m] + y_k^{P,pad}[m] + y_k^{N,pad}[m] \\ m = 0, 1, ..., L_{SYM}-1 \tag{27}$$

where

$$y_k^{DES}[m] = \sum_{n=\ell_1}^{\ell_2} x_k^c[n+\frac{L_f-1}{2}]\, \mathbf{a}_k[m+\frac{L_f-1}{2}-n] \tag{28}$$

$$y_k^{P,pad} = \big[(y_k^P)^T, \quad (0_{(L_{SYM}-1-\frac{L_f-1}{2})\times 1})^T\big]^T \tag{29}$$

$$y_k^{N,pad} = \big[(0_{(L_{SYM}-1-\frac{L_f-1}{2})\times 1})^T, \quad (y_k^N)^T\big]^T \tag{30}$$

where in turn

$$\ell_1 = \max\{-\frac{L_f-1}{2},\, m-L_f+1\},$$
$$\ell_2 = \min\{m,\, L_{SYM}-1-\frac{L_f-1}{2}\}$$

$$y_k^P[m'-L_{SYM}-\frac{L_f-1}{2}] = \sum_{n=m'-L_f+1}^{L_{SYM}-1} x_k^{P,c}[n]\, \mathbf{a}_k[m'-n], \tag{31}$$
$$m' = L_{SYM}+\frac{L_f-1}{2}, ..., L_{SYM}+L_f-2,$$

$$y_k^N[m'] = \sum_{n=0}^{m'} x_k^{N,c}[n]\, \mathbf{a}_k[m'-n], \quad m' = 0, ..., \frac{L_f-1}{2}. \tag{32}$$

In (31) and (32), $x_k^{P,c}$ and $x_k^{N,c}$ denote the CP-appended previous and next f-OFDM symbols respectively. Then, according to (8), the subband signals are added to form $y[m]$, upconverted and transmitted.

Similarly to (27)–(32), the signal at the front-end of the receiver can be separated to desirable and ISI components with the difference that the ISI length due to the channel does not extend that of the subband filter but partially overlaps and amplifies it (see Fig. 2). After subband filtering and before DFT operation, the k-th subband receives a mixture of the desired signal and interference terms which can be written as [5]

$$\bar{y}_k[m] = \bar{y}_k^{DES}[m] + \bar{y}_k^{N,pad}[m] + \bar{y}_k^{P,pad}[m] + \bar{y}_k^{ACI}[m] + \bar{y}_k^{ICI}[m] \\ + \bar{\eta}_k[m], \quad m = 0, ..., L_{SYM}-1. \tag{33}$$

B. Interference terms

For the ISI term due to the previous symbol we can write

$$\bar{y}_k^{P,pad} = [(\bar{y}_k^P)^T, (0_{(L_{SYM}-1-\frac{L_f-1}{2})\times 1})^T]^T, \tag{34}$$

[5]The statistical properties of the interference components are not affected by the following CP removal and DFT operation.

where

$$\bar{y}_k^P[m] = \sum_{n=-\frac{L_f-1}{2}+1}^{0} \mathbf{a}_k^*[m+\frac{L_f-1}{2}-n] \sum_{m'=\ell_1}^{\ell_2} \mathbf{h}_k^P[n-m'+\frac{L_f+L_{h,k}-2}{2}] y_k^P[m'+\frac{L_{h,k}-1}{2}] \,, \quad (35)$$

$$m = 0, ..., \frac{L_f-1}{2}-1,$$

$$\ell_1 = \max\{-\frac{L_{h,k}-1}{2}, n-L_{h,k}+1+\frac{L_f-1}{2}\}$$

$$\ell_2 = \min\{n+\frac{L_f-1}{2}, \frac{L_f+L_{h,k}-2}{2}-1\}$$

where in turn, $\mathbf{h}_k^P$, corresponding to $\mathbf{H}_k^P$, represents the effective CIR pertained to the ISI component by the previous f-OFDM symbol and y_k^P is given by (31). Similar equations are obtained for the ISI component corresponding to the next f-OFDM symbol.

To connect the received ISI components to the input f-OFDM symbols, we can use (31) and (32) in (35) and its dual obtained for the next f-OFDM symbol. This implies that each ISI component signal, $\bar{y}_k^P[m]$ or $\bar{y}_k^N[m]$, is the result of summation over many terms each including a data symbol weighted by the corresponding CIR and subband filter taps. Data symbols are assumed independent and identically distributed. As such, according to the central limit theorem, it can be shown that each symbol of the ISI component in (33) approximately follows a Gaussian distribution with zero mean, an approximately diagonal covariance matrix and variance of $\sigma_{ISI}^2 \approx \|\mathbf{a}_k\|^4 \left(\left\|\mathbf{h}_k^P\right\|^2 + \left\|\mathbf{h}_k^N\right\|^2\right) \sigma_{x_k}^2/(L_f^2 L_{h,k})$.

For the ACI component in the received symbols, we can adopt the same approach as in the ISI component analysis to obtain an exclusive time domain relationship between the input data symbols and the output ACI component. Comparing the matrix-vector equation of the ACI (14) with that of the ISI in (11)–(13), we observe that the ACI component is composed of a summation over an even higher number of terms each of which contain a data symbol from another subband. As such, it is more convincing to invoke the central limit theorem and approximate the ACI component in the output symbols by a Gaussian distribution with zero mean, an approximately diagonal covariance matrix where the variance can be shown to be of the form $\sigma_{ACI}^2 \approx (K-1)\|\mathbf{a}_k\|^4 \left(\left\|\mathbf{h}_k^1\right\|^2 + \left\|\mathbf{h}_k^2\right\|^2 + \left\|\mathbf{h}_k^3\right\|^2\right) \sigma_{x_k}^2/(L_f^2 L_{h,k})$, where $\mathbf{h}_k^1$, $\mathbf{h}_k^2$, and $\mathbf{h}_k^3$ are the CIRs corresponding to $\mathbf{H}_k^1$, $\mathbf{H}_k^2$, and $\mathbf{H}_k^3$ respectively. As observed in [3], the ACI power reduces remarkably by increasing the filter length with the case of $L_f = \frac{N}{2}$ incurring the lowest ACI power. In addition, one should note that the ACI term is significantly lower when different subbands are synchronized, which is the case in this work. Nevertheless, even in such cases the ACI term exists due to the non-orthogonality between subbands.

Following (17), similarly to ISI and ACI, the ICI contribution in each received symbol results from a 3 level summation over many terms each including an input symbol. Thus, according to the central limit theorem, we can show that the ICI contribution can also be approximated as a complex Gaussian sequence with zero mean, approximately diagonal covariance matrix and variance of $\sigma_{ICI}^2 \approx \frac{L_O-L_{CP}}{N+L_O} \|\mathbf{a}_k\|^4 \left(\left\|\mathbf{h}_k^C\right\|^2\right) \sigma_{x_k}^2/(L_f^2 L_{h,k})$ where $\mathbf{h}_k^C$ is the corresponding CIR to $\mathbf{H}_k^C$. Furthermore, in a general case with asynchronous subbands, the ACI power is the greatest with the ISI and ICI power being the second and the third respectively. Nonetheless, in contrast to the ACI and ICI, the ISI power is not reduced significantly by increasing the CP length and hence has the most adverse effect on the system in a general case [3].

Finally, for the covariance of subband noise contribution at two symbol locations we can write

$$\mathbb{E}\{\bar{\eta}_k[m']^* \bar{\eta}_k[m]\} \approx \|\mathbf{a}_k\|^2 \sigma_\eta^2. \quad (36)$$

Since the CP removal and DFT operation do not alter the covariance of the subband noise, assuming normalized T and D_k, the covariance of the subband noise vector n_k at two f-OFDM symbols reads as

$$\mathbb{C}_{n_k} = \mathbb{E}\{n_{k,u} n_{k,v}^H\} \approx \Psi_k \Psi_k^H \mathbb{E}\{\eta_{k,u} \eta_{k,v}^H\} \quad (37)$$

$$= D_k^H T T^H D_k \mathbb{E}\{\bar{\eta}_{k,u} \bar{\eta}_{k,v}^H\} = M^2 \|\mathbf{a}_k\|^2 \sigma_\eta^2 \mathbf{I}_M. \quad (38)$$

where $\Psi_k = D_k^H T A_k^H$.

C. Estimation derivation

Letting $\Phi_k = A_k R D_k E_k$, from (3)–(7), (9)–(14) and (17), the received f-OFDM symbol at the k-th subband can be represented as

$$\begin{aligned} \bar{Z}_k &= \bar{Z}_k^{DES} + \bar{Z}_k^{ISI} + \bar{Z}_k^{ACI} + \bar{Z}_k^{ICI} + n_k \\ &= \Psi_k \mathbf{H}_k^C \Phi_k X_k + \Psi_k \mathbf{H}_k^P \Phi_k X_k^P + \Psi_k \mathbf{H}_k^N \Phi_k X_k^N + \\ &\quad \Psi_k \sum_{i=1, i\neq k}^{K} (\mathbf{H}_k^1 \Phi_i X_i^N + \mathbf{H}_k^2 \Phi_i X_i^C + \mathbf{H}_k^3 \Phi_i X_i^P) + \\ &\quad \bar{Z}_k^{ICI} + \Psi_k \eta_k \end{aligned} \quad (39)$$

which provides a framework to derive the impairment source estimator. As such, following the observation of [3] that in contrast to ICI and ACI which rapidly vanish by increasing the CP length, the ISI term does not significantly decrease (see Fig. 7 of that reference), herein, we incorporate the ISI effect into the estimator and following the statistical properties of other interference terms in Section III-B approximate their additive effect as a Gaussian sequence with a diagonal covariance matrix. Therefore,

$$v_k = \bar{Z}_k^{ACI} + \bar{Z}_k^{ICI} + n_k \quad (40)$$

$$\mathbb{C}_{v_k} \approx (\sigma_{ACI}^2 + \sigma_{ICI}^2 + \sigma_{n_k}^2) \mathbf{I}_M. \quad (41)$$

Hence,

$$\begin{aligned} \bar{Z}_k &\approx \bar{Z}_k^{DES} + \bar{Z}_k^{ISI} + v_k \\ &= \Psi_k \mathbf{H}_k^C \Phi_k X_k + \Psi_k \mathbf{H}_k^P \Phi_k X_k^P + \Psi_k \mathbf{H}_k^N \Phi_k X_k^N + v_k \end{aligned} \quad (42)$$

By using $y_k^{DES} = \Phi_k X_k$, $y_k^P = \Phi_k X_k^P$ and $y_k^N = \Phi_k X_k^N$ and rearranging the convolution operation, we can write

$$\bar{Z}_k \approx \Psi_k (Y_k^P \mathbf{h}_k^P + Y_k^{DES} \mathbf{h}_k^C + Y_k^N \mathbf{h}_k^N) + v_k \quad (43)$$

where Y_k, Y_k^P, and Y_k^N represent the Toeplitz convolution matrices obtained from their corresponding vectors as previously done for the channel vector. Applying (41) in a similar way

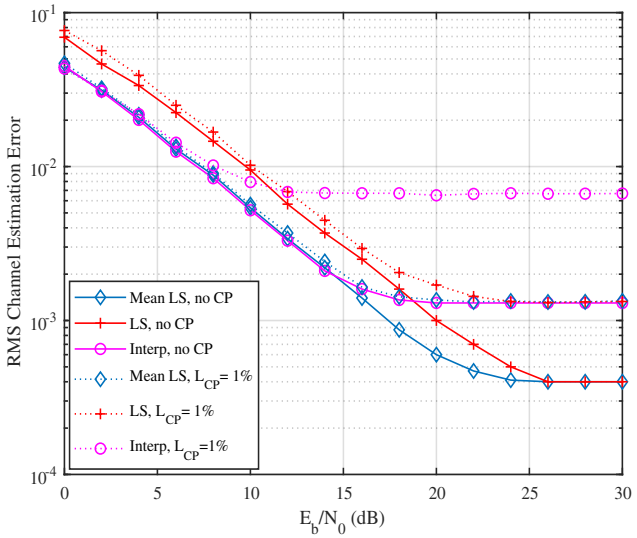

Fig. 3: RMS of channel estimation error for different methods with no CP and 1% CP length versus input E_b/N_0 values

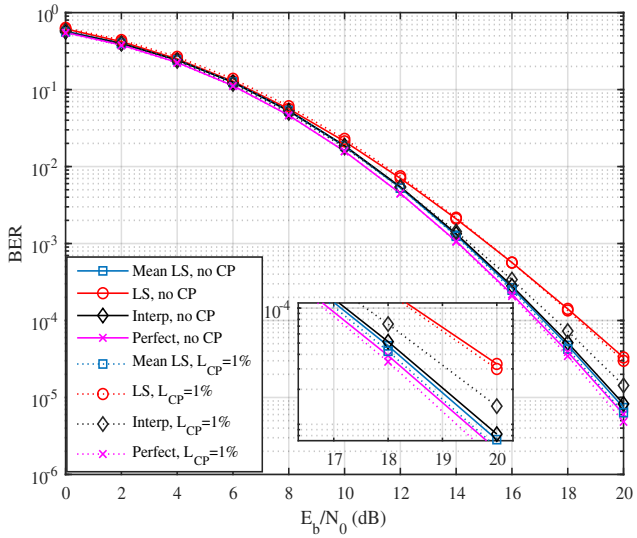

Fig. 4: BER of the f-OFDM transceiver for perfect channel and estimated channels in zero and 1% CP length versus input E_b/N_0 values

to [6]–[8], the maximum likelihood criterion is simplified to a linear equation where, up to an additive constant term, the resulting LS equation in the matrix form can be written as

$$\bar{Z}_k \approx \Psi_k \mathbf{Y}_k \mathbf{\Lambda}_k = \mathbf{\Gamma}_k \mathbf{\Lambda}_k \tag{44}$$

where

$$\begin{aligned} \mathbf{\Gamma}_k &= \Psi_k \mathbf{Y}_k \\ \mathbf{Y}_k &= [Y_k^P,\ Y_k^{DES},\ Y_k^N] \\ \mathbf{\Lambda}_k &= [(\mathbf{h}_k^P)^T,\ (\mathbf{h}_k^C)^T,\ (\mathbf{h}_k^N)^T]^T. \end{aligned} \tag{45}$$

Hence, the channel estimate can be obtained by

$$\hat{\mathbf{\Lambda}}_k = \mathbf{\Gamma}_k^{\dagger} \bar{Z}_k \tag{46}$$

where the operator $[.]^{\dagger}$ represents the Moore-Penrose pseudo inverse computed as $\mathbf{\Gamma}_k^{\dagger} = (\mathbf{\Gamma}_k^H \mathbf{\Gamma}_k)^{-1} \mathbf{\Gamma}_k^H$. Varying the parameter L_s between its limits, $L_{k,h}$ and $L_f - L_{k,h}$, shapes the different parts of the Toeplitz convolution matrices of the channel, reflecting the assumed ISI plus noise contribution level from neighboring symbols. Consistently, empirical experiments show that in low signal to noise ratio per bit (E_b/N_0) and high frequency selectivity, higher L_s and in high E_b/N_0 and lower frequency selectivity, lower L_s values attain lower error rates. What is finally extracted as being the estimated CIR in subband k is the central part, $\hat{\mathbf{h}}_k^C$ out of which the desired total channel $\hat{\mathbf{h}_C}$ can be shaped by per-subband fast Fourier transform (FFT) taking, concatenation and a total IFFT.

IV. Simulation Results

As implemented, the f-OFDM transceiver contains $N = 1200$ subcarriers split into $K = 100$ subbands each consisting of $M = 12$ subcarriers. Subcarrier spacing is 15 KHz. The estimation is performed by Monte Carlo simulations of transmitting one burst during which the channel is assumed invariant. A burst of length $L_p = 7$ is adopted where the

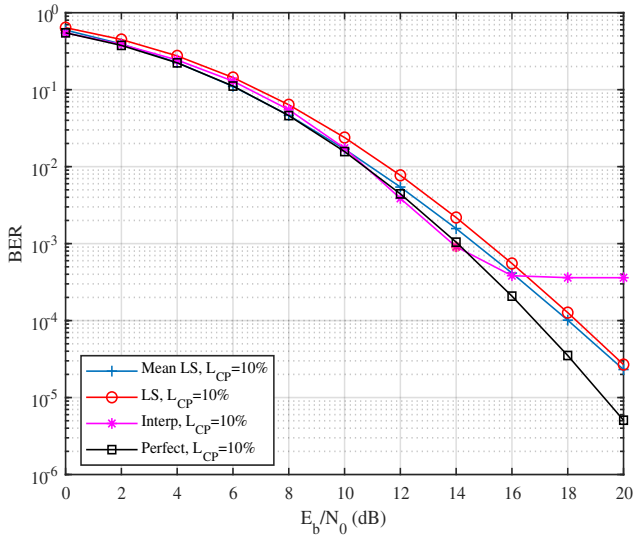

Fig. 5: BER of the f-OFDM transceiver for perfect channel and estimated channels in 10% CP length versus input E_b/N_0 values

1st, 3rd and 7th time indexes comprise of merely data and the rest contain a pilot tone in every 4 subcarriers. The input bit sequence is coded by a turbo code of approximate rate $R = 1/2$ before QPSK modulation and transmission. The applied channel follows the Jakes fading type using the EVA channel model parameters. The deployed prototype filter is a hamming-windowed truncated sinc whose parameters are chosen empirically to provide a good frequency localization as observed by the frequency response and the error rate values in additive white Gaussian noise (AWGN) channel conditions. The range of L_s value pertained to the proposed method

is empirically chosen based on the level of the frequency selectivity of the channel while its precise value in the range does not enormously impact the estimation result.

In Fig. 3, the root mean square of the channel estimation error for the proposed estimator is depicted compared to a linear interpolation-based pilot-to-pilot estimator. In both configurations of the proposed method, i.e. with and without repeating and averaging over the 4 pilot vectors, less error floor is visible in high E_b/N_0 values. In low values thereof, however, the estimation based on only one pilot time index suffers performance degradation as compared to the other two methods both of which utilize averaging over 3 pilot time indexes. Moreover, all of the methods result in lower error values throughout the SNR range when no CP is available. This can be explained by the slight randomness that originates from the slight perturbation caused by the lower CP value which in turn aids the estimation and interpolation task by the increased diversity. The performance gap of the two CP configurations is specially higher in the linear interpolation method.

Fig. 4 depicts the bit error rate (BER) values of the f-OFDM transceiver system with the proposed estimators as compared to the interpolation-based method and the perfect channel in two CP configurations, i.e. the CP length of zero and 1% as compared to N. The equalization task is performed by the zero-forcing one-tap-per-subcarrier scheme in all cases. It can be seen that the error rates of the two configurations perform very closely. In addition, the proposed average-taking LS method performs nearly as good as the perfect channel. It however, shows a significant performance loss when the averaging is not implemented. Moreover, the only method that results in remarkably lower error rates in higher CP length value is the one based on interpolation. This indicates the robustness of the proposed estimation method against a low CP length, which combined with a careful design of the prototype filter in terms of frequency localization, leads to the potential to save on the overall spectral efficiency of the transceiver.

Finally, increasing the CP length in steps of 1% to values as high as 10%, which, for our prototype filter, approximately equals that of the original f-OFDM proposal [4] as the width of the main lobe of the prototype filter in time samples, did not provide a significant improvement in terms of channel estimation error or BER results. As an example, the BER result for the case of $L_{CP} = 10\%$ is illustrated in Fig. 5. Although this should be further studied in various scenarios, one can conclude that, at least in moderately frequency-selective environment considered herein, not only the removal of the CP does not degrade the system performance significantly, but the considerable spectral efficiency gain of up to 7-10% makes it an appealing choice.

V. Conclusion

In this work, specific signal model of f-OFDM was analyzed in order to craft a specific channel estimation for such transceivers. Based on the properties of the interference terms, an LS-type pilot-based channel estimation method and a variant of it that includes averaging over the f-OFDM symbols, were proposed that outperform the pilot-to-pilot interpolation-based method which also made use of the averaging over pilot vectors. In addition, the results indicated that, by carefully designing the prototype filter, shortening or removing the CP becomes possible, which in turn, ends in a significant improvement of the spectral efficiency of the f-OFDM transceiver compared to the existing works where the minimum required CP length for a satisfactory performance in identical experimental conditions is reported multiple times higher than that considered in this work.

References

[1] R. Gerzaguet *et al.*, "The 5G candidate waveform race: a comparison of complexity and performance," *EURASIP Journal on Wireless Communications and Networking*, vol. 2017, no. 1, pp. 13, Jan 2017.

[2] X. Zhang, M. Jia, L. Chen, J. Ma and J. Qiu, "Filtered-OFDM - enabler for flexible waveform in the 5th generation cellular networks," in *2015 IEEE Global Communications Conference (GLOBECOM)*, Dec 2015, pp. 1–6.

[3] L. Zhang, A. Ijaz, P. Xiao, M. Molu and R. Tafazolli, "Filtered OFDM systems, algorithms, and performance analysis for 5G and beyond," *IEEE Transactions on Communications*, vol. 66, no. 3, pp. 1205–1218, March 2018.

[4] J. Abdoli, J. Ming, and J. Ma, "Filtered OFDM: A new waveform for future wireless systems," in *IEEE 16th International Workshop on Signal Processing Advances in Wireless Communications (SPAWC)*, June 2015, pp. 66–70.

[5] J. Choi, D. J. Love and P. Bidigare, "Downlink raining Techniques for FDD Massive MIMO Systems: Open-Loop and Closed-Loop Training With Memory," *IEEE Journal of Selected Topics in Signal Processing*, vol. 8, no. 5, pp. 802–814, Oct 2014.

[6] A. Baghaki and B. Champagne, "Joint carrier frequency offset, sampling time offset and channel estimation for OFDM-OQAM systems," in *VTC*, Boston, MA, USA, Sep. 2015.

[7] A. Baghaki and B. Champagne, "Joint frequency offset, time offset, and channel estimation for OFDM/OQAM systems," *EURASIP Journal on Advances in Signal Processing*, vol. 2018, no. 1, pp. 4, Jan 2018.

[8] A. Baghaki and B. Champagne, "Joint carrier frequency offset, sampling time offset and channel estimation in multiuser OFDM/OQAM systems," *2018 IEEE Wireless Communications and Networking Conference (WCNC)*, pp. 1–6, 2018.